Demonstration of air-guided quantum cascade lasers without top claddings

V. Moreau[1], M. Bahriz[1], R. Colombelli[1], R. Perahia[2], O. Painter[2], L. R. WIlson[3], A. B. Krysa[4]

[1]*Institut d'Electronique Fondamentale, Université Paris Sud, CNRS, 91405 Orsay, France*
[2]*Department of Applied Physics, California Institute of Technology, Pasadena, California 91125, USA*
[3]*Department of Physics and Astronomy, University of Sheffield, Sheffield S3 7RH, UK*
[4]*EPSRC Centre for III-V Technology, University of Sheffield, Sheffield S3 7RH, UK*

Abstract: We report on quantum cascade lasers employing waveguides based on a predominant air confinement mechanism in which the active region is located immediately at the device top surface. The lasers employ ridge-waveguide resonators with narrow lateral electrical contacts only, with a large, central top region not covered by metallization layers. Devices based on this principle have been reported in the past; however, they employed a thick, doped top-cladding layer in order to allow for uniform current injection. We find that the in-plane conductivity of the active region - when the material used is of high quality - provides adequate electrical injection. As a consequence, the devices demonstrated in this work are thinner, and most importantly they can simultaneously support air-guided and surface-plasmon waveguide modes. When the lateral contacts are narrow, the optical mode is mostly located below the air-semiconductor interface. The mode is predominantly air-guided and it leaks from the top surface into the surrounding environment, suggesting that these lasers could be employed for surface-sensing applications. These laser modes are found to operate up to room temperature under pulsed injection, with an emission spectrum centered around $\lambda \approx 7.66\ \mu m$.

OCIS codes: (140.5960) Semiconductor lasers; (140.3070) Infrared and far-infrared lasers; (140.3410) Laser resonators

References and links

1. J. Faist, F. Capasso, D. L. Sivco, C. Sirtori, A. L. Hutchinson, A. Y. Cho, "Quantum cascade laser," Science **264**, 553 (1994).
2. C. Gmachl, F. Capasso, D. L. Sivco, and A. Y. Cho, "Recent progress in quantum cascade lasers and applications," Rep. Progr. in Physics **64**, 1533 (2001).
3. J. Faist and C. Sirtori, in '*Long wavelength infrared semiconductor lasers*' (J. Wiley and Sons, Hoboken, NJ, USA, 2004).
4. M. Beck, D. Hofstetter, T. Allen, J. Faist, U. Oesterle, M. Ilegems, E. Gini, H. Melchior, "Continuous Wave Operation of a Mid-Infrared Semiconductor Laser at Room Temperature," Science **295**, 301 (2002).
5. J. S. Yu, S. Slivken, A. Evans, L. Doris, and M. Razeghi, "High-power continuous-wave operation of a 6 μm quantum-cascade laser at room temperature," Appl. Phys. Lett. **83**, 2503 (2003).
6. M. Troccoli, D. Bour, S. Corzine, G. Hofler, A. Tandon, D. Mars, D. J. Smith, L. Diehl, and F. Capasso, "Low-threshold continuous-wave operation of quantum-cascade lasers grown by metalorganic vapor phase epitaxy," Appl. Phys. Lett. **85**, 5842 (2004).
7. G. Wysocki, M. McCurdy, S. So, D. Weidmann, C. Roller, R. F. Curl, and F.K. Tittel, "Pulsed Quantum-Cascade Laser-Based Sensor for Trace-Gas Detection of Carbonyl Sulfide," App. Opt. **43**, 6040 (2004).

#85011 - $15.00 USD Received 10 Jul 2007; revised 21 Aug 2007; accepted 21 Aug 2007; published 26 Oct 2007

8. A. A. Kosterev and F. K. Tittel, "Chemical sensors based on quantum cascade lasers," IEEE J. Quantum Elec. **38**, 582 (2002).
9. D. Erickson, T. Rockwood, T. Emery, A. Scherer, and Demetri Psaltis, "Nanofluidic tuning of photonic crystal circuits," Proc. SPIE **6475**, 647513 (2007).
10. B. Maune, M. Loncar, J. Witzens, M. Hochberg, T. Baehr-Jones, D. Psaltis, A. Scherer, and Y. Qiu, "Liquid-crystal electric tuning of a photonic crystal laser," Appl. Phys. Lett. **85**, 360 (2004).
11. M. Loncar, A. Scherer, and Y. Qiu, "Photonic crystal laser sources for chemical detection," Appl. Phys. Lett. **82**, 4648 (2003).
12. C. Monat, P. Domachuk, and B. J. Eggleton, "Integrated optofluidics: A new river of light," Nature Photon. **1**, 106 (2007).
13. D. Psaltis, S. R. Quake, and C. Yang, "Developing optofluidic technology through the fusion of microfluidics and optics," Nature **442**, 381 (2006).
14. M. Schaden, A. Doninguez-Vidal, and B. Lendl, "Simultaneous measurement of two compounds in aqueous solution with dual quantum cascade laser absorption spectroscopy," Appl. Phys. B **83**, 135 (2006).
15. M. Loncar, B. G. Lee, L. Diehl, M. A. Belkin, F. Capasso, M. Giovannini, J. Faist, and E. Gini, "Design and fabrication of photonic crystal quantum cascade lasers for optofluidics," Opt. Express **15**, 4499 (2007).
16. J. Chen, Z. Liu, C. F. Gmachl, and D. L. Sivco, "Silver halide fiber-based evanescent-wave liquid droplet sensing with room tempreature mid-infrared quantum cascade lasers," Opt. Express **13**, 5953 (2005).
17. C. Charlton, A. Katzir, and B. Mizaikoff, "Infrared Evanescent Field Sensing with Quantum Cascade Lasers and Planar Silver Halide Waveguides," Anal. Chem. **77**, 4398 (2005).
18. R. Perahia, K. Srinivasan, O. Painter, V. Moreau, M. Bahriz, R. Colombelli, F. Capasso, "Quantum cascade photonic crystal lasers: design, fabrication, and applications," CLEO 2006 (CTuAA5), Long Beach CA, May 2006.
19. R. Perahia, O. Painter, M. Bahriz, V. Moreau, R. Colombelli, "Design of quantum cascade lasers for intra-cavity sensing in the mid infrared," *manuscript in preparation*.
20. R. Perahia, O. Painter, V. Moreau, M. Bahriz, R. Colombelli, L.R. Wilson, A.B. Krysa, "Quantum Cascade Microdisk Lasers for Mid Infrared Intra-Cavity Sensing," CLEO 2007 (CTuE5), Baltimore (MA), May 2007.
21. L. Diehl, B.G. Lee, P. Behroozi, M. Loncar, M.A. Belkin, F. Capasso, T. Aellen, D. Hofstetter, M. Beck, and J. Faist, "Microfluidic tuning of distributed feedback quantum cascade lasers," Opt. Express **14**, 11660 (2006).
22. R. Colombelli, K. Srinivasan, M. Troccoli, O. Painter, C.F. Gmachl, D. M. Tennant, A. M. Sergent, D. L. Sivco, A. Y. Cho, F. Capasso, "Quantum Cascade Surface-Emitting Photonic Crystal Laser," Science **302**, 1374 (2003).
23. D. Hofstetter, T. Aellen, M. Beck, and J. Faist, "High average power first-order distributed feedback quantum cascade lasers," IEEE Photon. Technol. Lett. **12**, 1610 (2000).
24. W. Schrenk and N. Finger and S. Gianordoli and L. Hvozdara and G. Strasser and E. Gornik, "Surface-emitting distributed feedback quantum-cascade lasers," Appl. Phys. Lett. **77**, 2086 (2000).
25. C. Sirtori and C. Gmachl and F. Capasso and J. Faist and D. L. Sivco and A. L. Hutchinson and A. Y. Cho, "Longwavelength ($\lambda \approx 8-11.5$ μm) semiconductor lasers with waveguides based on surface plasmons," Opt. Lett. **23**, 1366 (1998).
26. M. Bahriz, V. Moreau, J. Palomo, R. Colombelli, D.A. Austin, J.W. Cockburn, L.R. Wilson, A.B. Krysa, J.S. Roberts, "Room temperature operation of $\lambda \approx 7.5$ μm surface-plasmon quantum cascade lasers," Appl. Phys. Lett. **88**, 181103 (2006).
27. M.A. Ordal, L.L. Long, R.J. Bell, S. E. Bell, R. R. Bell, R.W. Alexander, and C. A. Ward, "Optical properties of the metals Al, Co, Cu, Au, Fe, Pb, Ni, Pd, Pt, Ag, Ti, and W in the infrared and far infrared," App. Opt. **22**, 1099 (1983).
28. V. Moreau, M. Bahriz, J. Palomo, L.R. Wilson, A.B. Krysa, C. Sirtori, D.A. Austin, J.W. Cockburn, J.S. Roberts, R. Colombelli, "Optical Mode Control of Surface-Plasmon Quantum Cascade Lasers," Photon. Technol. Lett. **18**, 2499 (2006).
29. A.B. Krysa, J.S. Roberts, R.P. Green, L.R. Wilson, H. Page, M. Garcia, and J.W. Cockburn, "MOVPE-grown quantum cascade lasers operating at $\approx$ 9 μm wavelength," J. Cryst. Growth, **272**, 682 (2004).
30. R. P. Green, L. R. Wilson, E. A. Zibik, D. G. Revin, J. W. Cockburn, C. Pflügl, W. Schrenk, G. Strasser, A. B. Krysa, J. S. Roberts, C. M. Tey, and A. G. Cullis , "High-performance distributed feedback quantum cascade lasers grown by metalorganic vapor phase epitaxy," Appl. Phys. Lett. 85, 5529 (2004).
31. The commercial software *Comsol Multiphysics* was used.
32. Z. Yin, and F. W. Smith, "Optical dielectric function and infrared absorption of hydrogenated amorphous silicon nitride films: Experimental results and effective-medium-approximation analysis," Phys. Rev. B **42**, 3666 (1990).
33. L. A. Coldren, S. W. Corzine, "Diode Lasers and Photonic Integrated Circuits," Wiley-Interscience (1995).
34. V. Moreau, M. Bahriz, R. Colombelli. P.-A Lemoine, Y. De Wilde, L.R. Wilson, and A.B. Krysa, "Direct imaging of a laser mode via midinfrared near-field microscopy," Appl. Phys. Lett. **90**, 201114 (2007).

#85011 - $15.00 USD Received 10 Jul 2007; revised 21 Aug 2007; accepted 21 Aug 2007; published 26 Oct 2007

1. Introduction

The quantum cascade (QC) laser [1] has proven to be a promising mid-infrared and THz laser source. It can efficiently cover the first and second atmospheric windows [2, 3], an important wavelength range for chemical and bio-sensing, and for free-space optical communications. In particular the performances of these devices have rapidly progressed, thanks to improved material properties and to the use of more advanced processing/packaging techniques [4, 5, 6].

QC lasers are now used as laser sources in conventional spectroscopic setups for gas detection [7, 8], and their characteristic high power and single mode operation have allowed the demonstration of detection capabilities down to the ppb (part-per-billion). The possibility of performing intra-cavity spectroscopy or sensing [9, 10, 11, 12, 13, 14, 15, 16, 17] with quantum cascade lasers is an alternative intriguing approach [18, 19, 20, 21]. In such a scheme, the laser would react to a material (gas, fluid, or solid particles) deposited within or on the surface of the laser by detuning its emission wavelength or increasing its threshold current density. There are a variety of laser cavity geometries that are amenable to such intra-cavity sensing. These include porous photonic crystal laser structures[9, 10, 11, 15, 22], edge-sensitive microdisk and microring lasers[19], or top-surface-sensitive devices in which the optical mode leaks above the semiconductor surface[21, 23, 24]. While the former approach involving photonic crystals can theoretically provide the highest sensitivity, since the intra-cavity region is accessible through the photonic-crystal holes, these structures also are more difficult to fabricate. In addition, for many applications where QC laser intra-cavity spectroscopy would be most interesting, such as in the analysis of chemical or biological macromolecules in fluids, room-temperature (RT) operation is highly desirable as this would allow for sensing of a much wider variety of substances in their natural state. The top-surface-sensitive laser approach, although providing a smaller sensitivity, is much less challenging to fabricate.

A simple strategy to obtain leakage of the optical mode from the top surface of the device is to employ a waveguide where the laser optical mode is guided by the top air-semiconductor interface (see Fig. 1). The top surface must not be covered by metal, but the current has to be injected into the devices, possibly through narrow lateral contacts (see Fig. 2). Previous devices that employed this architecture made use of thick top, doped semiconductor claddings in order to provide uniform current injection [23, 24]. However, the use of top cladding layers limits the amount of optical field that extends above the device surface. In order to enhance the surface-sensitivity, the QC lasers studied in this work are formed from semiconductor heterostructures originally designed for operation as surface-plasmon lasers, with no top cladding layers. The peculiarity of this approach is that the same heterostructure can be processed as a surface-plasmon QC laser [25, 26], if the metal contacts cover the whole surface of the device, or as an air-confinement device, if only narrow lateral contacts are deposited and the top surface is left exposed. The transition between these two regimes is smooth. If *most* of the device top surface is metal coated, then the mode will be *mostly* plasmonic. On the other hand, if *most* of the device top surface is left exposed - as in our case - then the mode will be *mostly* air-guided. For this work we decided to employ narrow lateral contacts in order to (i) reduce the propagation losses and (ii) maximize the amount of energy that leaks out of the device top surface.

The outline of the paper is as follows. In section 2 we describe the modal properties of the laser modes using a one-dimensional transfer matrix model. More detailed finite-element method (FEM) simulations of the waveguide laser structure (as well as of edge-sensitive microdisk and micro-ring lasers) will be presented in a separate theoretical paper[19]. Section 3 details the fabrication and characterization of the laser structure, and in section 4 we describe several tests used to positively identify the laser mode as the dominantly air-guided mode of the laser structure. Finally, we conclude in section 5 by summarizing the results and discussing the potential applications of such devices.

#85011 - $15.00 USD Received 10 Jul 2007; revised 21 Aug 2007; accepted 21 Aug 2007; published 26 Oct 2007

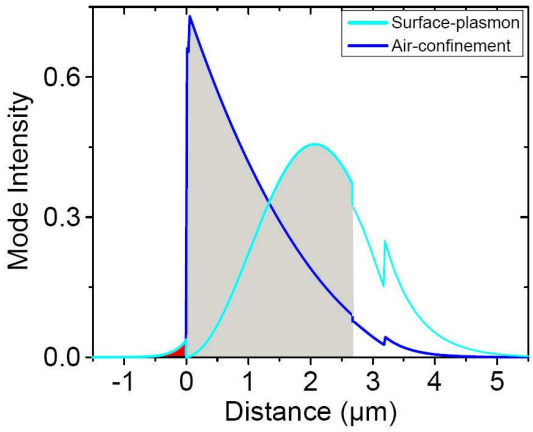

Fig. 1. Waveguide calculations, performed in a 1D transfer matrix approach, for two different waveguide geometries applied to the same heterostructure. Dark blue-line: surface-plasmon waveguide mode with a gold plasmon-carrying layer ($\Gamma = 90\%$, $\alpha = 48\ cm^{-1}$). Light blue-line: air-confinement waveguide with removal of the top n^+-layers ($\Gamma = 72\%$, $\alpha = 3\ cm^{-1}$). The grey areas correspond to the laser active region. The surface is located at $x = 0$ and the red area is the portion of the mode that leaks evanescently above the surface. Its "confining" factor Γ_{air} is $\approx 0.9\%$.

2. Waveguide design

The layer sequence of the QC laser structure studied in this work is shown in Table 1. The two waveguide solutions, air-guided and surface-plasmon, of this laser structure are summarized in Fig. 1 and are thoroughly discussed in a separate theoretical paper[19]. The figure shows a 1D simulation, performed within a transfer-matrix approach, for these two geometries. We consider a typical QC laser active region, $\approx 2.6\ \mu$m thick, sandwiched between a 0.5-μm-thick InGaAs bottom cladding layer (n-doped 5x10^{16} cm^{-3}), and thin (10 nm n=10^{19} cm^{-3}, 40 nm n=10^{17} cm^{-3}) top contact-facilitating layers. The whole structure is grown on a highly-doped InP substrate, capped with a 2-μm-thick low-doped (1x10^{17} cm^{-3}) InP buffer. The dielectric constants for the doped semiconductor layers were calculated using a Drude-Lorentz model, while the values for the metals were taken from Ref. [27].

Table 1. QCL Epitaxy

Material	Doping (cm^{-3})	Thickness (Å)
GaInAs	1×10^{19} [n^{++}]	100
GaInAs	1×10^{17} [n]	400
Active region	-	2.635×10^4
InGaAs	5×10^{16} [n]	5000
InP	1×10^{17} [n]	2×10^4
InP substrate	5×10^{18} [n]	2.5×10^6

In the first case (surface-plasmon waveguide), metallic contacts are deposited on the whole device surface. It is well known that a metal-semiconductor interface can sustain surface-plasmon waves [25, 26, 28]. The resulting waveguide mode is shown in Fig. 1 (dark blue curve).

#85011 - $15.00 USD Received 10 Jul 2007; revised 21 Aug 2007; accepted 21 Aug 2007; published 26 Oct 2007

A confinement factor (Γ) of 90% and a value of 48 cm^{-1} for the losses (α) are obtained if a gold surface-plasmon carrying layer [26] is employed. No penetration of the mode above the device surface is to be expected if the top metal is not patterned, since the skin depth (δ_s) is extremely short. We estimate in fact $\delta_s \approx 10$ nm for gold at a wavelength $\lambda = 8$ μm.

In the second case (air-confinement waveguide), the mode is guided at the semiconductor-air interface. An evanescent electric field is to be expected on the top surface of these devices (Fig. 1), since a portion of the laser mode (Γ_{air}) leaks out evanescently from the device top surface. A 1D calculation yields $\Gamma = 72\%$ and $\alpha = 33$ cm^{-1}. However the losses are largely induced by the thin, highly doped n+ layers on the top surface of the device. If the 100-Å-thick n$^+$-top-layer is removed (as usually happens during device processing), the resulting confinement factors and losses become $\Gamma = 72\%$, and $\alpha = 3$ cm^{-1}. Taking into account the mirror losses for a typical resonator length of 1.5 mm, the air-confinement waveguide should exhibit a figure of merit approximatly 4 times better than a surface-plasmon waveguide. Note, however, that a 1D calculation inevitably underestimates the losses for an air-confinement waveguide, since it does not include the presence of the lateral (lossy) metallic contacts.

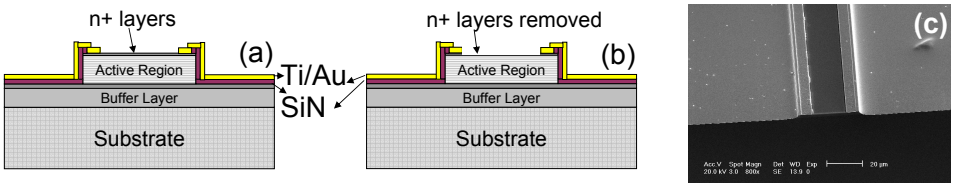

Fig. 2. (a) Schematic layout of the fabricated devices. The contacts are deposited laterally on the edge of the ridge waveguide. Most of the ridge surface is left exposed to the air. The sidewalls in the real-devices are slanted, not vertical, since a wet chemical etch ($HBr:HNO_3:H_2O$) has been used. (b) A wet etch, or an aggressive oxygen plasma followed by a dip in HCl can remove the thin top n$^+$ layer. (c) SEM image of a typical final device.

3. Device fabrication and characterization

The laser heterostructure (sample MR2230) was grown by low pressure metal organic vapor phase epitaxy (MOVPE), using an $In_{0.53}Ga_{0.47}As/Al_{0.48}In_{0.52}As$ lattice matched to a highly-doped InP substrate. Further details of the growth process can be found in [29]. The active regions are based on a 2-phonon-resonance design (Ref. [30]), with the lasing transition designed for nominal emission at $\lambda = 7.5$ μm. Fifty active-region/injector stages were grown, preceded by a 500-nm-thick InGaAs layer doped to n =5x10^{16} cm^{-3} and followed by InGaAs contact facilitating layers.

For this work, the laser structure has been processed in a Fabry-Perot ridge geometry with only narrow lateral contacts. An HBr-based wet chemical etch has been used to define the laser resonators. A large portion of the device surface is left exposed, as shown in Fig. 2(c). The fabrication procedure is sketched in Figs. 2(a) and 2(b). Lasers with waveguide ridge widths of 26, 31, 36, and 41 μm, and nominal air-gap opening widths of 16, 21, 26, and 31 μm, were fabricated. The thin, highly doped top contact layer can be removed either by wet chemical etch, or by RIE (Fig. 2(b)). However, the top contact layer gets most probably removed during the surface cleaning of the sample with oxygen plasma followed by de-oxydation with HCl/HF, making the final etch-procedure described above often unnecessary. After mechanical polishing and back contact deposition (Ti/Au - 10/120 nm), the samples are cleaved into laser bars, mounted with indium solder on copper blocks, wire-bonded and loaded in a cryostat for device characterization.

#85011 - $15.00 USD Received 10 Jul 2007; revised 21 Aug 2007; accepted 21 Aug 2007; published 26 Oct 2007

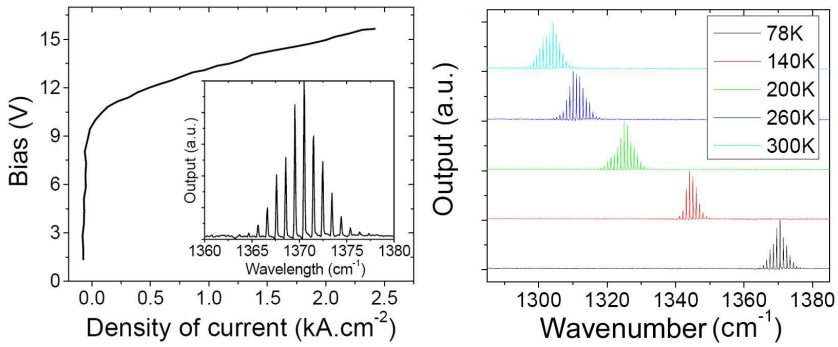

Fig. 3. (a) Current-voltage (IV) characteristics at a temperature of 78K for a typical device (100 ns pulse width at 5 kHz repetition rate). The device dimensions are 1500 μm X 36 μm. Inset: Fabry-Perot spectrum of a typical device at 78 K. (b) Emission spectra at different temperatures for a typical device (50 ns pulse width at 84 kHz repetition rate). The spectra were acquired with a Fourier Transform Infrared Spectrometer (FTIR) operated in rapid-scan mode and with a resolution of 0.125 cm^{-1}. The signal was detected with a DTGS (deuterated triglycine sulfate) detector.

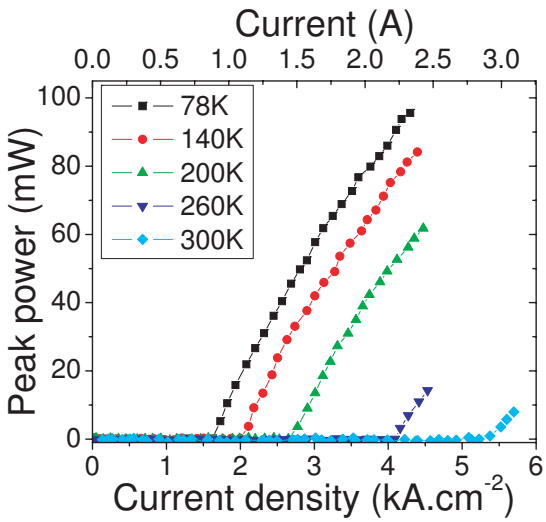

Fig. 4. Light-current (LI) characteristics of a typical device at different temperatures (100ns pulse width at 1 kHz repetition rate). The device dimensions are 1500 μm X 36 μm. The power was measured with a fast MCT (Mercury-Cadmium-Telluride) detector that had been calibrated with a thermopile.

Figure 3(a) shows the current-voltage (IV) characteristics of a typical device. Its sharp turn-on is evidence that the current is efficiently injected, and that the contribution of the thin, top n^+ layers to the lateral current spreading is not essential. In fact, the inherent lateral conductivity of the active region dominates the current spreading process, with measurements on test-structures fabricated from the same wafer yielding an effective lateral current spreading extent of 20-25 μm[28]. We found that efficient current injection can be achieved (as determined by laser threshold) in laser ridges with widths as wide as 41 μm (corresponding to an air gap of 31 μm), provided that two lateral top contacts are used. If current is injected from one of the two top

#85011 - $15.00 USD Received 10 Jul 2007; revised 21 Aug 2007; accepted 21 Aug 2007; published 26 Oct 2007

contacts only, the maximum device operating temperature drops (from RT to 250K).

The light-current (LI) characteristics of a 36-μm-wide device is reported in Fig. 4. The device achieves lasing in pulsed-mode up to room temperature. The peak output power is $\approx$ 100 mW at 78K, and $\approx$ 10 mW at 300K. Finally, Fig. 3(b) reports typical laser emission spectra for different operating temperatures. At a temperature of 78 K the emission is peaked at $\lambda = 7.3$ μm, while at 300K the emission is detuned by 0.4 μm, up to $\lambda = 7.7$ μm. The devices exhibit clear Fabry-Perot fringes (Fig. 3), which yield an effective index of refraction $n_{\text{eff}} = 3.41$ at $T = 78$ K, and an $n_{\text{eff}} = 3.44$ at RT.

4. Mode identification

Two-dimensional waveguide simulations show that, in principle, a laser mode exists that is completely guided by the lateral metal bands used for current injection (see Fig. 5(b) and Ref.[19]). On one hand this mode exhibits much higher propagation losses than the predominantly air-guided mode (Fig. 5(c)). On the other hand, it benefits from a better current injection given that it is located exactly below the metallic contact bands. It is necessary to exclude that this mode is excited in the current devices.

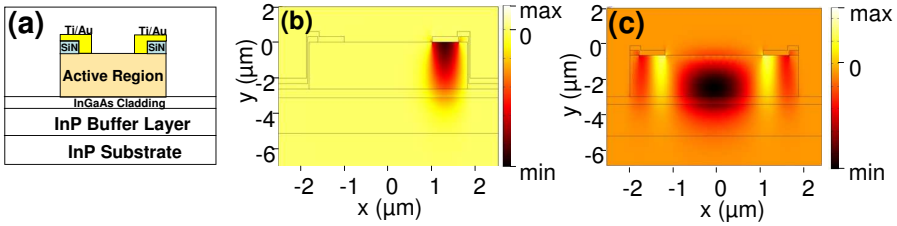

Fig. 5. (a) Schematic geometry of the measured device. (b) High-loss waveguide mode (E_z component) localised below one of the metal bands. We calculate $\alpha \approx 52\ cm^{-1}$ for this mode. An identical mode exists and it is localised below the other metal band. (c) Low-loss, air-guided modes (E_z component) for a laser device with ridge width of 36 μm. The geometry corresponds to panel (a). We calculate $\alpha \approx 9\ cm^{-1}$ for this mode.

Two tests were performed to achieve this goal: the emission far-field of a typical air-confinement laser fabricated for this work was characterised and compared with realistic 2D numerical simulations, and a Ti/Au metal deposition with a very thick (and therefore lossy) Ti sticking layer was employed. The results of the two tests - which are described in detail below - indicate that the optical mode is predominantly guided at the air-semiconductor interface.

Two-dimensional numerical simulations of the waveguide mode were performed using a finite-elements solver [31]. The detailed device geometry used for the simulations, reported in Fig. 5(a), has been deduced from SEM images of the fabricated devices. The index of refraction of the semiconductor layers was obtained with a simple Drude-Lorentz model, while the values for the metal and for the SiN layers were taken from Refs. [27] and [32], respectively.

The simulations provide the value of the electric field across a longitudinal cross-section of the device end-facet. Under the approximation that this is identical to the electric field distribution outside the facet, the laser far-field emission pattern can be obtained *via* the following formula[33]:

$$|\mathbf{E}_{far}(\theta_x,\theta_y,R)|^2 = \frac{\cos^2(\theta_x)\cos^2(\theta_y)}{\lambda^2 R^2(\sin^2(\theta_x)\sin^2(\theta_y))}\left|\int\int |\mathbf{E}(x,y)|e^{+ikx\cdot sin(\theta_x)}e^{+iky\cdot sin(\theta_y)}dxdy\right|^2, \quad (1)$$

#85011 - $15.00 USD Received 10 Jul 2007; revised 21 Aug 2007; accepted 21 Aug 2007; published 26 Oct 2007

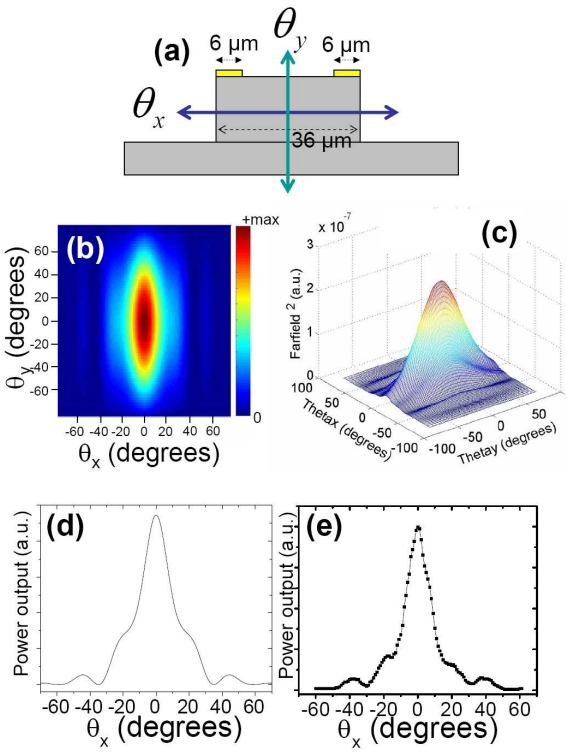

Fig. 6. (a) Cross-section schematic of the end-facet of the laser ridge. The ridge width is 36 μm. (b) 2D color-plot of the calculated far field for the ridge in panel (a). (c) 2D surface-plot of the calculated far field intensity. (d) Calculated far field as a function of θ_x (see panel a), for $\theta_y = 0$ (e) Experimental far field, measured by scanning a liquid-nitrogen-cooled MCT detector in front of the device at a fixed distance. The agreement with the calculated far field is excellent

.

where $\mathbf{E}$(x,y) is the electric-field vector at the position x,y on the laser facet; $\mathbf{E}_{far}(\theta_x,\theta_y,R)$ is the electric field vector in the device far-field at a distance R and angles θ_x,θ_y as defined in Fig. 6(a); λ is the vacuum wavelength and $k = \frac{2\pi}{\lambda}$.

Figure 6(b) shows the calculated device far-field as a 2D color-plot. The θ_x angular direction contains information on the lateral structure of the optical mode. In fact, the 1D sections of the far-field pattern obtained at fixed θ_y are not single peaked, but they are instead structured, as it is evident from the 2D surface-plot of the calculated far-field (see Fig. 6(c)). A 1D far-field pattern calculated at $\theta_y = 0$ (Fig. 6(d)) is compared to the experimental result (Fig. 6(e)) obtained by performing a θ_x scan of the detector while keeping $\theta_y = 0$. The agreement is excellent, and it strongly suggests that the measured laser mode is that of the predominantly air-guided mode in the simulations reported in Fig. 5(c). Note: the structured far-field emission pattern is a trace of the mode hybrid nature. In fact, a mode that is localized below the air-semiconductor or metal-semiconductor interface only would not give rise to such oscillations, but it would instead produce a simple Gaussian-like far-field profile.

Additional evidence that the actual lasing mode is not guided by the lateral metal contact layers as in Fig. 5(b), is that the devices studied in this work were fabricated using Ti/Au metal contacts deposited by radio-frequency sputtering. We have previously observed that such metal layers, when used for creating surface-plasmon QC lasers, introduce a significant amount of ad-

#85011 - $15.00 USD Received 10 Jul 2007; revised 21 Aug 2007; accepted 21 Aug 2007; published 26 Oct 2007

ditional optical loss, due to the difficulty of controlling the deposition of very thin (few tens of Angstroms) Ti layers, thus preventing lasing action in such devices. The fact that the measured devices in this case have relatively low threshold currents and high operating temperatures, is again another indication that the metal contact layers are not significantly involved in waveguiding of the laser mode, and that the laser mode is indeed predominantly guided in the uncovered air-gap region of the laser ridge, as in Fig. 5(c).

5. Conclusions

In conclusion, we implemented quantum cascade lasers with air-guided modes on structures where the active region is immediately at the surface of the devices. The lasers operate up to 300K, in pulsed mode, with peak output powers of ≈ 10 mW. The analysis of the temperature, spectral and far-field behavior confirms the results of the numerical simulations.

The leakage of the optical mode from the top surface of the devices represents a useful degree of freedom towards the development of laser devices that are sensitive to a material or a fluid deposited on their top surface. An example application is that of intra-cavity spectroscopy or sensing with QC lasers for the detection of fluids and their constituents. Initial sensing experiments with fluids will target the identification of common solvents like isoproponal and ethanol. The evanescent electric field at the device surface could be also directly observed with near-field microscopy techniques[34], transforming the QC laser into a local probe.

In general, the ability to laterally electrically inject QC surface-sensitive laser devices is of importance for the creation of a variety of laser geometries, in particular microcavity lasers such as microdisks and photonic crystals. The lack of top metal contacts allows the semiconductor etch *via* dry-etching without the problem of metal re-deposition inside the photonic-crystal holes. At the same time, the reduced epitaxial thickness will not require a deep semiconductor etch, which is often a challenging technological issue. Finally, these devices are *dual-use*: two different waveguide geometries (air-guided ans surface-plasmon) could be simultaneously implemented on the same laser heterostructure.

Acknowledgments

We thank C. Faugeras for help with the far-field measurements; F. Julien, C. Sirtori, O. Demichel for useful discussions, and J. Palomo for technical help. This work was conducted as part of a EURYI scheme award (www.esf.org/euryi). The Caltech portion of this work was supported by the DARPA Center for Optofluidics (http://www.optofluidics.caltech.edu). This work is supported by the UK Engineering and Physical Sciences Research Council (EPSRC) and by the Royal Society. The device fabrication has been performed at the nano-center "Centrale Technologique Minerve" at the Institut d'Electronique Fondamentale.

#85011 - $15.00 USD Received 10 Jul 2007; revised 21 Aug 2007; accepted 21 Aug 2007; published 26 Oct 2007